Modeling Climate and Tectonic Controls on Bias in Measured River Incision Rates

Clarke DeLisle[1] and Brian J. Yanites[1]

[1] Department of Earth and Atmospheric Sciences, Indiana University

Corresponding author: Brian J. Yanites (byanites@iu.edu)

Key Points:

- We present a numerical model that reproduces biases in rates of river incision measured from strath terraces
- We find that these measurement biases are the strongest when climates are highly variable and rock uplift is slow
- Understanding bedrock incision measurement biases allows for bias correction in field studies and improves data comparability

Abstract:

Rates of land surface processes provide insights into climate and tectonic influences on landscape dynamics. River incision rates into bedrock are estimated by dating perched landforms such as strath terraces, assuming a constant bedrock incision rate from terrace abandonment to present. These estimates express biases from the stochastic nature of river incision and from using a mobile channel elevation as a reference frame. No existing mechanistic framework fully addresses these biases. We introduce a 1-D river evolution model incorporating fluvial mechanics, sediment dynamics, tectonics, and climatic factors to predict these biases and assess their sensitivity to climate and rock-uplift rate. Findings suggest biases intensify under highly variable climates and slow rock uplift, with the period of climate being a primary control. Our

model improves river incision measurement reliability, impacting paleoclimate and tectonic geomorphology reconstructions.

Plain Language Summary

Geomorphologists often measure how fast rivers erode bedrock over time by dating river terraces that have been uplifted to be higher than the elevation of the modern river channel. This helps us learn how landscapes evolve and about what past climates were like over long timescales. But this method is complicated by the fact that rivers do not erode rocks at a steady rate and the elevation of the channel surface above which we measure terrace height changes over time. We present a numerical model that predicts how these terraces develop under different climates and rates of rock uplift. Our model shows how these factors affect our measurements of river incision and that they are most impactful when climates are highly variable and rock uplift is slow. Our model helps us make better measurements of river erosion and understand how climate and rock uplift shape landscapes.

1. Introduction

Strath terraces are planar surfaces that are abandoned as rivers incise into bedrock (Schanz et al., 2018). These landforms preserve valuable records of river incision (Craddock et al., 2010; Rittenour, 2008; Stock et al., 2005; Wegmann & Pazzaglia, 2002), tectonic forcing (Yanites et al., 2010) and climate change (Gran et al., 2013). Studies of river incision commonly use depositional ages of fluvial sediments capping strath terraces and elevation above the modern channel to calculate rates of incision. These measurements are, however, plagued by a bias in which younger landforms may yield spurious higher incision rates (Finnegan et al., 2014; Gardner et al., 1987). The strength of these biases varies widely in landscapes around the world

(Nativ & Turowski, 2020), but no framework exists to predict and correct for these biases mechanistically. The observed biases have been explained by a combination of the long-tailed distribution of incision hiatus durations (Finnegan et al., 2014) and the use of a dynamic channel elevation as a reference frame (Gallen et al., 2015). Yet, the importance of these drivers and their dependence on climate and tectonics is unconstrained.

Strath terraces are created by cyclical aggradation, planation, and river incision in active landscapes (Hancock & Anderson, 2002). In Figure 1**,** we show a schematic representation of the cyclicity which leads to terrace abandonment. During periods of low transport capacity (relative to sediment supply), sediment covers bedrock and slows or stops vertical bedrock erosion. During these periods, at-a-station channel elevation increases at the rate of rock uplift. While this is occurring, channels move laterally and plane broad bedrock surfaces known as straths. When climate shifts to a higher relative transport capacity, sediment transport rates increase, and channels resume eroding bedrock, abandoning strath terraces. Variable erosional hiatuses and varying channel reference frames are posited to both lead to the observed biases in river incision rates (Finnegan et al., 2014; Gallen et al., 2015).

Here we present a numerical model of 1-D bedrock river evolution which captures episodic aggradation and river incision, terrace abandonment, and incision hiatuses. Our model accounts for the impacts of both weather and climate while incorporating stochastic sediment supply and dynamic channel width. We evolve our model to equilibrium over 10^6 model years and document terrace preservation, reproducing measurement biases in rates of river incision. We test our model under different climate and tectonic regimes and find that the bias is strongest when rock uplift is slow and climate is highly variable. A mechanistic model accounting for these forcings is critical to disentangling climate and tectonic controls on fluvial landscape

evolution and furthers the utility of strath terraces as records of landscape evolution and climate change.

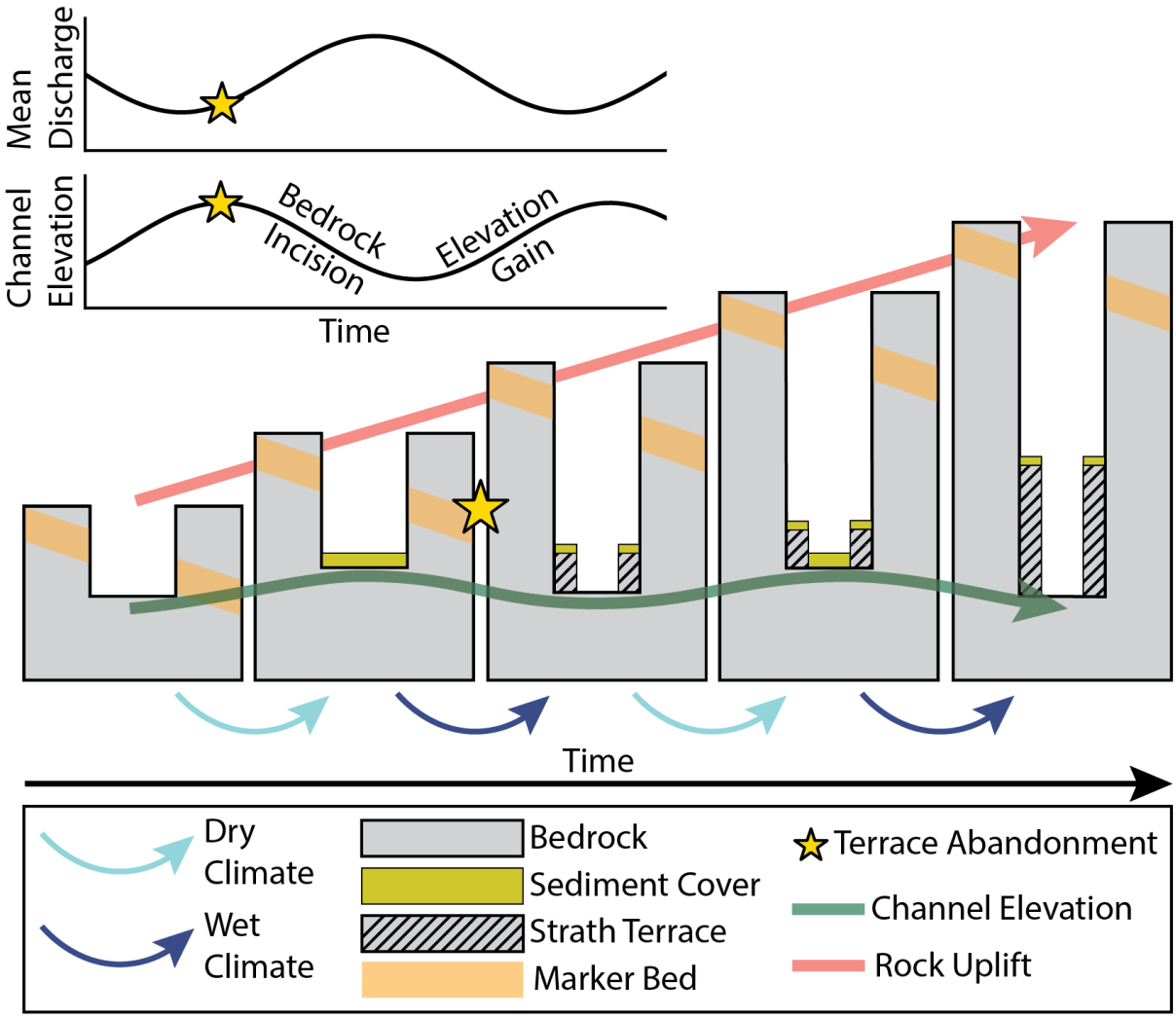

Figure 1. Mechanistic understanding of terrace genesis. During periods of dry climate, rivers receive less water thus their capacity to transport sediment and incise bedrock is decreased. Sediment aggrades further shielding bedrock from erosion during these periods. As rock uplift is constant through time in our modeling framework, the elevation of the bedrock channel increases when bedrock is shielded from erosion. Although we do not explicitly model lateral channel motion, we assume that during these periods of aggradation the channel moves laterally and planes off a strath. When the climate shifts from dry to wet, sediment transport rates increase, aggraded sediment is removed, and rivers resume bedrock incision. At these shifts is when we predict strath terraces to be abandoned. Repeated climate cycles after terrace abandonment increase the height of strath terraces. Through time, the local elevation of the bedrock channel is cyclical in response to these climate cycles (green line).

2. Model Mechanics

2.1 Overview

We model the evolution of channel bed elevation and incorporate impacts of stochastic water discharge, stochastic hillslope sediment supply, channel width changes, and vertical bedrock erosion (DeLisle & Yanites, 2023; B. J. Yanites, 2018). While the model is a 1-D river profile, periods of erosional hiatus are assumed to promote the planation processes (Hancock & Anderson, 2002), leading to strath terrace formation. River discharge is drawn from a modified inverse gamma distribution (Crave & Davy, 2001; Deal et al., 2018; DiBiase & Whipple, 2011; Lague et al., 2005; Molnar et al., 2006). Sediment delivery varies with river discharge while keeping long-term sediment supply constant, equal to the product of the contributing drainage area upstream and the rate of rock uplift. We evolve bed sediment following the Exner equation (Exner, 1925; Paola & Voller, 2005) and bedload sediment transport is calculated using an excess shear stress model (Meyer-Peter & Müller, 1948; Wong & Parker, 2006). Bedrock erosion occurs in our model using a stream power relationship and accounting for the shielding effect of sediment cover (Sklar & Dietrich, 2001; Whipple et al., 2000a). When the channel is fully covered with sediment, no bedrock erosion occurs. Bedrock erosion increases linearly with degree of bedrock exposure.

We investigate the impact of climate on our model by varying mean discharge through geomorphic time; mean river discharge varies following an imposed sinusoid with a period which we vary from 20Kyr to 120Kyr. To capture differences in climate oscillation strength, we vary the amplitude of the variation from 10% to 60%. At a given timestep (2 weeks) in our model, we draw nondimensional water discharge from our inverse gamma distribution (representing stochastic weather events) and scale this discharge by the long-term mean

discharge (representing long timescale climate patterns). Model parameters are described in the next section.

2.2 Channel Elevation and Bedrock Erosion

The elevation ($z_{channel}$) of each node in our model river evolves from the competition between rock uplift (U_r) and bedrock erosion (E)

$$\frac{\partial z_{channel}}{\partial t} = \begin{cases} U_r - E & when\ h = 0 \\ U_r + \frac{\partial h}{\partial t} & when\ h > 0 \end{cases} \qquad Eq.\ 1$$

where h is the thickness of bedload sediment overlying bedrock in each model node. Bedrock incision is modeled using a modified stream power law which accounts for the cover effect of immobile sediment.

$$E = FK\tau_b^a \qquad Eq.\ 2$$

Here, K is rock erodibility, a is a constant equal to 1 (Whipple et al., 2000b), τ_b is basal shear stress, and F is fractional bedrock exposure which varies from zero (a bed fully buried by sediment) to 1 (a channel with fully exposed bedrock) and depends on the ratio of sediment supply to transport capacity (Sklar & Dietrich, 2004).

2.3 Stochastic Water Discharge

We model stochastic river discharge with a modified inverse gamma distribution of nondimensional daily water discharge (Qw^*). We chose this distribution as it captures the rarity of both extreme low and high discharge values, can easily be tuned to change river discharge variability, and has been used in many studies of the impact of discharge variability on bedrock channel evolution and morphology (Crave & Davy, 2001; DiBiase & Whipple, 2011; Lague et al., 2005). The continuous probability distribution of nondimensional daily discharge is:

$$PDF_{\bar{Q}w,k_v}(Qw^*) = \frac{{k_v}^{k_v+1}}{\Gamma(k_v+1)} exp(-\frac{k_v}{Qw^*}) Qw^{*-(2+k_v)} dQw^* \quad \textit{Eq. 3}$$

where k_v controls discharge variability. For all models presented here we use k_v = 0.3, but this parameter can be calibrated with river gauging data.

2.4 Sediment Supply

The rate of rock uplift controls the long-term average bedload sediment supply rate to a landscape (assumed to be 30% of total sediment load); however, bedload sediment supply from hillslopes to rivers is temporally variable. This is especially true in steep, tectonically active landscapes where landslides are prevalent (Campforts et al., 2022; Marc et al., 2019). To capture this, we vary sediment supply linearly with flood frequency (DeLisle and Yanites, 2023). Nondimensional sediment (Qs^*) delivery scales linearly with nondimensional river discharge (Eq. 3). So that

$$Qs^* = Qw^* \quad \textit{Eq. 4}$$

We use nondimensional discharge, which represents the probability of an event of a given magnitude, rather than mean river discharge, to isolate the impact of climate on the capacity of rivers to move sediment and erode rock without varying long-term averaged sediment supply from hillslopes to channels. In our framework, a 100-year flood is always accompanied by the same volume of sediment, irrespective of whether climate is in a wet or dry period. This approach ensures that sediment supply is equal to the upstream rock uplift rate over geomorphically relevant timescales, regardless of current climate state.

2.5 Climate

We impose a sinusoidal oscillation in mean river discharge with periods that varies from 20kyr to 120kyr in 20kyr increments. For each period, we model amplitudes from 10% to 60% of

mean river discharge in 10% increments. For example, if long-term average discharge at a node is equal to $100m^3/s$ and we impose a climate magnitude of 40%, mean discharge is equal to $60m^3/s$ during dry periods and $140m^3/s$ during wet periods.

2.6 Numerical Experiments

We vary rock uplift rates from 0.5mm/yr to 5mm/yr and allow our model rivers to evolve to equilibrium under periodic climate forcing, and then undergo repeated climate cycles once dynamic equilibrium is attained. We document terrace abandonments, measure rates of river incision over the lifespan of a single terrace, and show trends in age-elevation relationships and measured incision rates across flights of inset terraces.

3. Mechanistic Drivers of Incision Biases

Figure 2 illustrates how the model captures the cycle of terrace formation through periods of sediment aggradation and incision (rock uplift of 0.5 mm/yr and 80Kyr period at 40% for the illustrated model run). Figure 2A is a time series of river discharge for one node in the model river. The pink line shows climate cycles in which mean discharge varies by ±40% relative to the long-term mean. The scatter around this line results from stochastic weather events, modeled using a modified inverse gamma distribution.

Figure 2B shows a time series of bedrock elevation and sediment cover at a node in our model river. We observe decreasing channel elevations relative to an unmoving datum during periods of wet climate, when sediment transport and bedrock erosion is elevated. Conversely, we see bedrock elevations increase when the climate is drier, as decreases in sediment transport capacity drive sediment aggradation which shields bedrock from mechanical weathering processes and allows rock uplift to outpace bedrock erosion. While not explicitly modeled, it is

during these periods that lateral channel motion, not channel width changes, plane off a wide strath surface that gets abandoned during wetter climates.

Figure 2C plots cumulative rock uplift vs cumulative incision. Cumulative incision increases quickly during wet climates, and stalls when sediment aggradation is high during dry climates. We predict the time at which terraces are abandoned by locating the local minima in cumulative incision detrended by cumulative rock uplift. We denote these times with yellow stars in Figure 2B and Figure 2C. We chose this metric because incision rate increases quickly after these local minima, and we suggest this as the time at which a river resumes bedrock incision and abandons a terrace. The elevation of these terraces is projected forward in time (gray dashed lines) at the rate of rock uplift (Figure 2B). The intercepts of these lines with the y-axis represent final terrace elevations.

Figure 2D shows the time series of incision rate that would be measured for a single terrace as it uplifts relative to an unmoving reference elevation (we use the channel elevation at the time of terrace abandonment). Here we document the incision hiatus bias, in which the measured rate of river incision decreases with terrace age, even with a stationary reference frame (Finnegan et al., 2014; Sadler, 1981). We note that the rate eventually overcorrects and underpredicts incision rates and eventually oscillates around the rate of rock-uplift, dampening with time.

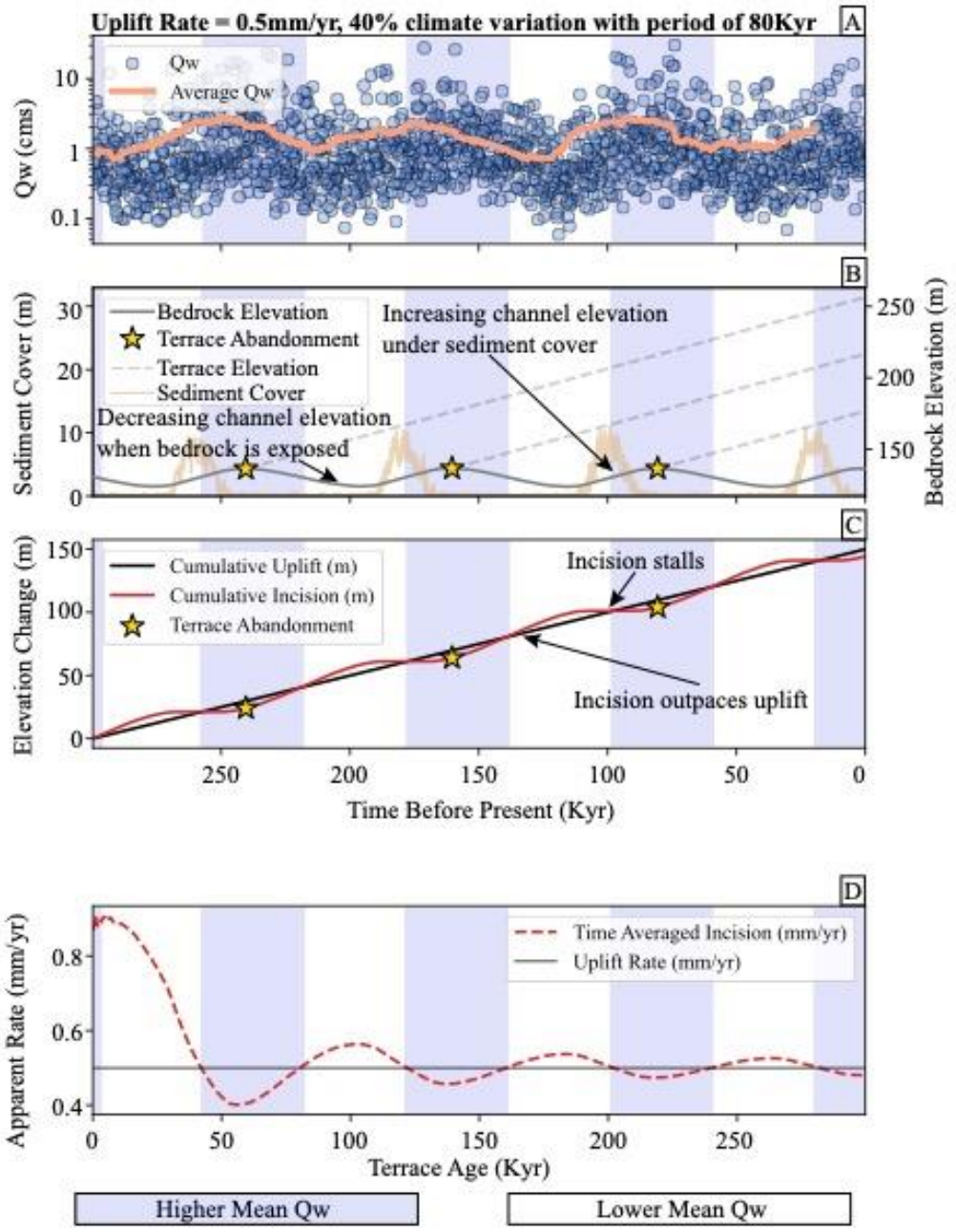

Figure 2. Time series of river discharge, channel morphology, and river incision during the development of a flight of strath terraces. All panels are colored to show times when climate (mean Qw) is increasing and decreasing. A) River discharge at one model node. Blue dots are stochastic discharge events, and the line is a moving average of river discharge. B) Time series of channel elevation and sediment cover. Dashed lines project terrace elevation following abandonment at yellow stars. C) Cumulative rock uplift and incision. Terraces are abandoned at times marked by yellow stars. D) Measurements of river incision through time for one uplifting strath terrace.

4. Model Terrace Flights

To document the presence of, and investigate controls on, the dynamic reference frame bias, we preserved flights of strath terraces over 250k model years at dynamic equilibrium for models across our parameter space. We show results from one such flight of terraces (Figure 3), where model parameters are the same as those described for Figure 2. Terrace elevations are calculated by projecting elevation growth at the rate of rock uplift once the terrace is abandoned (Figure 2).

We plot terrace ages vs terrace heights (Figure 3A). Terrace height is measured as the difference between the final terrace elevation and either the channel elevation at the time of terrace abandonment (gray points and line), the long-term mean channel elevation (dark green points and line), or the 5^{th} percentile value of channel elevation (light green points and line). These elevations are the elevation of the bedrock channel at a single node, which changes through time even at equilibrium in response to climate cycles (Figure 2B). We fit log-linear trends to flights of terraces using each method of terrace height measurement and report the slopes of these lines, normalized by the rate of rock uplift, (ß) in Figure 3A.

The gray points preserve the true rate of rock uplift and river incision following terrace abandonment, and so the slope of this line is equal to the rate of rock uplift (ß = 1.0). The dark green points and lines measure final terrace elevation above the long-term mean channel elevation which is lower than the channel elevation at the time of terrace abandonment, which occurs at local maxima in channel elevation (Figure 2B). This imparts a dynamic reference frame bias on our data, as the difference between mean channel elevation and channel elevation at the time of terrace abandonment represents a larger fraction of total terrace height for younger terraces than older terraces (Gallen et al., 2015). As such, ß = 0.89 when using mean channel

elevation. Using the 5th percentile elevation value increases the strength of the bias, where ß = 0.81.

We also calculate bedrock incision rates using each reference elevation described above and show that measured incision rates are higher over short time windows and when using a lower reference elevation (Figure 3B). This helps to explain the ubiquity of the biases in field measurements of bedrock incision, because if measurements are taken above a river channel that is in a period of incision (i.e., a period with significant exposed bedrock), our model predicts that the current channel elevation is lower than the channel elevation at the time of terrace abandonment, which generally occurs during a period of moderate sediment aggradation (Figure 2B).

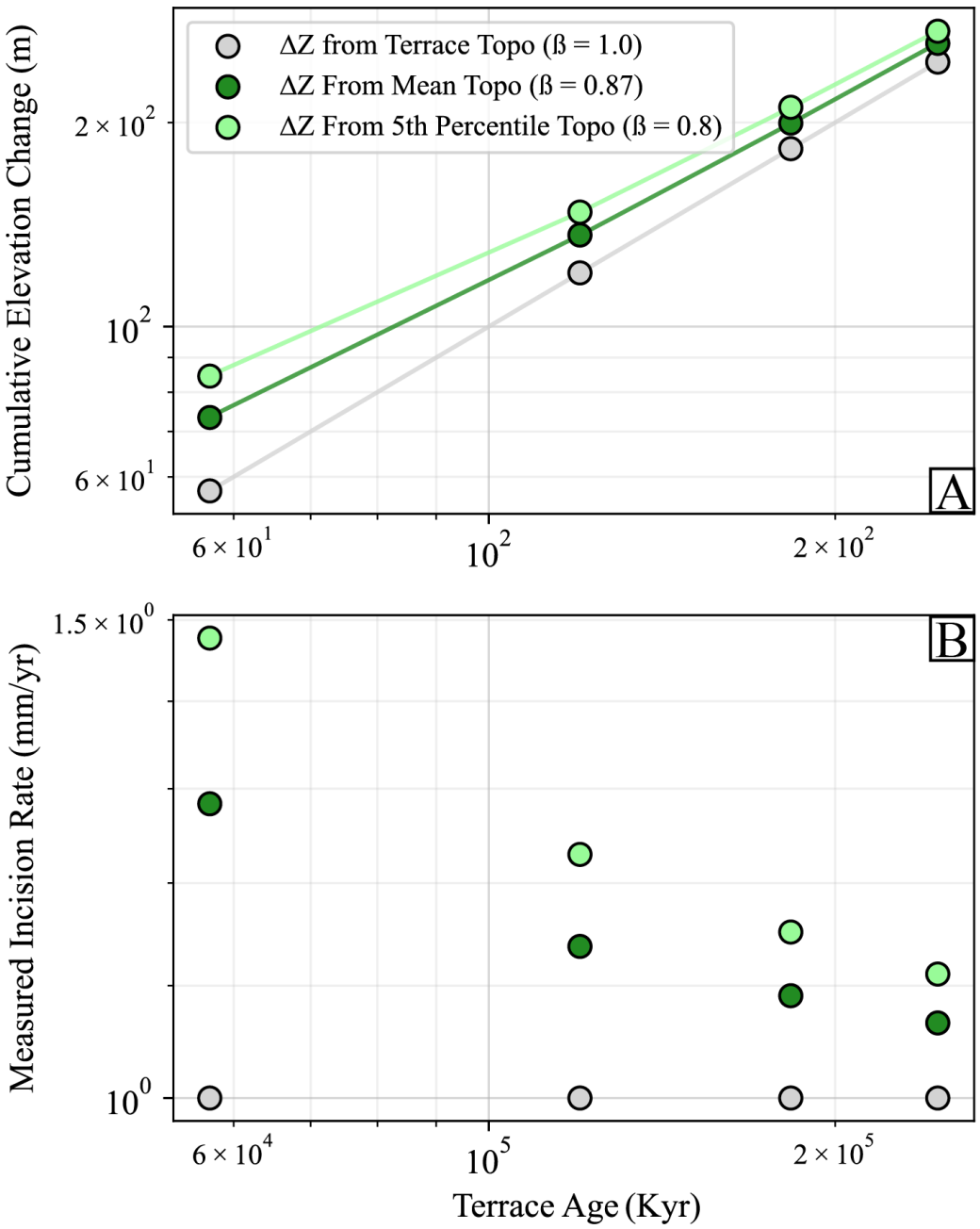

Figure 3. – Documenting dynamic reference frame bias in a flight of model river terraces. A) Terrace height vs age measured relative to the channel elevation at the time of terrace abandonment, the mean channel elevation, and the 5th percentile channel elevation. B) Rates of river incision for terraces of different ages measured using height above the three elevations listed above.

5. Factors Controlling Bias Strength

We document the combined impact of rock uplift rate, climate oscillation magnitude, and climate period on the strength of the dynamic reference frame bias (Figure 4). Each point represents the slope of a line fit to terrace age vs cumulative elevation change measurements (e.g. Figure 3A**)**. We use a reference frame that measures from the terrace elevation to the 5^{th} percentile channel elevation (i.e., light green points in 3A) for all measurements. We test the impact of changing rock uplift rate and climate oscillation magnitude by plotting data from models that covary rock uplift from 0.5mm/yr to 5mm/yr, climate oscillation magnitude from 10% to 60% of long-term mean discharge, and climate period from 20Kyr to 120Kyr.

Figure 4A shows the ß values for models run with a moderate rock uplift rate of 0.5mm/yr. Here we see that ß values decrease (biases are stronger) when climate variation is stronger and acts over longer time periods. The elevation of the bedrock channel, which we use as a reference frame for terrace height, is most variable in these scenarios with strongly varied climate over 120Kyr periods. Values of ß for this uplift rate range from 0.97 for a scenario with a 10% climate oscillation and a period of 20Kyr to 0.75 for a scenario with a 60% climate oscillation and a period of 120Kyr. ß values for a fast uplift rate of 5mm/yr document a similar trend (Figure 4B), where ß values are lowest with long-period and high-magnitude climate oscillation. Values of ß range from 0.89 to 0.99 for fast-uplifting models.

Our model predicts that dynamic reference frame biases in measurements of bedrock river incision rates are the strongest when rock uplift is slow and, thus, that measurements are more reliable in fast-uplifting landscapes. This occurs because terrace elevation above the active channel increases at the rock uplift rate once terraces are abandoned. In fast-uplifting landscapes, terraces quickly become tall, and so the measured terrace elevation is less impacted by the

dynamic elevation of the channel. In the slower uplifting models, the variability in channel elevation accounts for a larger fraction of total terrace height and thus imparts a stronger bias on measured incision rates.

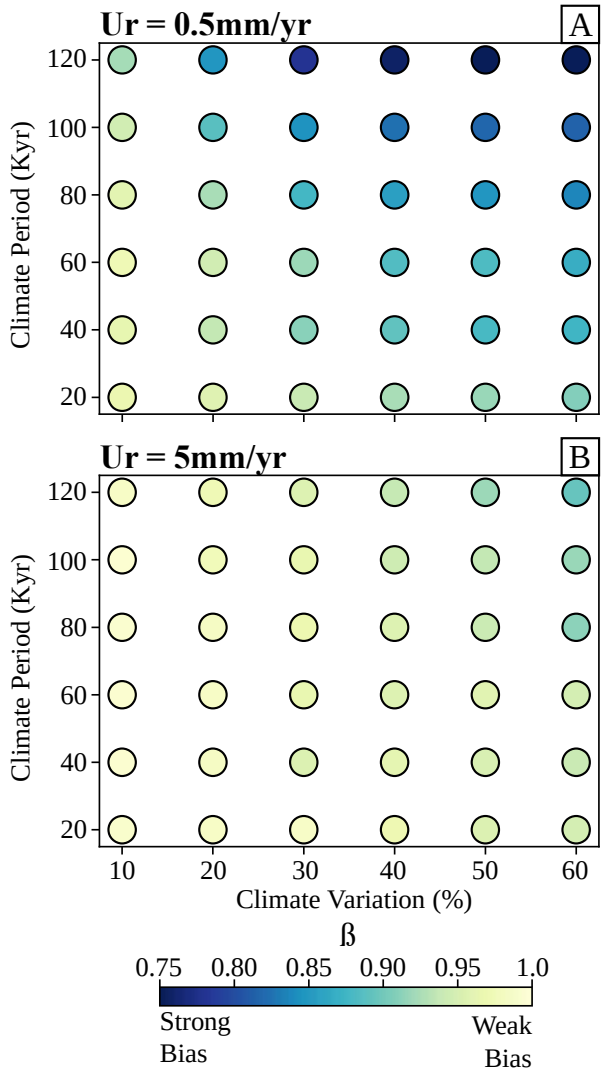

Figure 4. Relationships between magnitude of climate variation, climate variation period, and rate of rock uplift, strength of dynamic reference frame bias (ß). Lower values of ß occur when measured incision rate bias with measurement window is stronger. A) Results for Ur = 0.5mm/yr. B) Results for Ur = 5mm/yr. For both uplift rates, biases are strongest (ß values are lower) for longer and stronger climate oscillations. Biases are stronger under moderate rock uplift (5mm/yr) than fast rock uplift (5mm/yr).

6. Discussion

In this study, we present a numerical model that predicts the strength of measurement biases in rates of river incision by accounting for bedrock incision, sediment delivery and transport, tectonic rock uplift, and both weather and climate. Our model expands on conceptual models (Gallen et al., 2015), numerical models (Hancock & Anderson, 2002),and field observations (Finnegan et al., 2014; Gardner et al., 1987; Nativ & Turowski, 2020) and allows for interrogation of individual variables on the strength of these biases. This model is an important step towards understanding this widespread but enigmatic complicating factor in studies using rates of river incision from strath terraces.

Many modeling parameters that are important in controlling the dynamics of evolving bedrock rivers have been held constant across the model runs presented here to isolate the impact of climate variation on river incision measurement biases. Factors such as rock erodibility and grain size influence the slope of bedrock rivers, and variations in these parameters may yield different calculated values of ß as a result. Our dynamic width algorithm (Yanites, 2018) can be modified to allow for greater variations in channel width during periods of aggradation and incision. We refer the reader to Yanites (2018) for documentation of different bedrock incision rules (e.g. saltation-abrasion) within this modeling framework. While we vary the magnitude and period of our sinusoidal climate oscillation, we acknowledge that a simple sine wave is a simplified representation of real-world climate variations. While these parameters should be explored during efforts to calibrate our model to specific landscapes, we keep them constant for the purposes of this exploratory modeling study, and we do not believe that modifying them would detract from overall trends observed between rock uplift, climate oscillation, and the strength of measurement biases in rates of river incision.

The modeling framework presented in this paper links sediment delivery linearly with river discharge. We vary only river discharge over climate scales and not sediment supply to isolate the ability of a river to transport sediment and erode bedrock during repeated climate cycles, but we recognize that the relationships between climate change and sediment dynamics are complex and not well understood (Malatesta & Avouac, 2018). Future work should aim to disentangle these factors and improve our understanding of the effects of changes in long-term sediment supply which may overprint the effects described here.

Our model predicts terrace abandonment, marked by periods of increased vertical bedrock incision, which occurs when climates transition from dry (lower relative transport capacity) to wet (higher relative transport capacity); this is driven by an increase in capacity for both sediment transport and bedrock erosion due to higher bed shear stresses. Global datasets (Schanz et al., 2018) show, however, that the conditions that lead to strath planation and abandonment are diverse and variable. While we account for only one such mechanism here, many other factors such as long-term averaged sediment supply, rock uplift rate, and discharge variability are readily modified in our modeling framework and thus it could be used to examine a variety of mechanisms for terrace genesis.

The range of ß values that we predict using our modeling framework (from 0.75 to 0.99) is smaller than the range of ß values observed in global compilations, which range from <0.5 to >1.0 (Finnegan et al., 2014; Nativ & Turowski, 2020). There are two possible explanations for this mismatch. First, our model may underpredict the strength of biases because of the unchanging nature of sediment supply in response to climate shifts within our modeling framework. While we made this decision intentionally to isolate the impact of river discharge and capacity for sediment transport and erosion, further investigation of model predictions where

sediment supply is modulated by climate shifts alongside changes in river discharge may broaden the range of predicted ß values. Second, we present results from terraces that form while the model is in dynamic equilibrium. Global compilations of these biases may include landscapes in which local tectonics are transient, which would impart a stronger bias (lower ß values) than the ones we predict here.

Strath terraces are often used as markers of climate change in incising landscapes (Molnar et al., 1994; Tao et al., 2020; Wegmann & Pazzaglia, 2002), and inset strath terrace suites represent some of the best archives of past climates. However, understanding how terrace genesis results from combined climate, tectonic, and fluvial forces is critical to accurately interpreting climatic signals from terraces. Our model presents a significant step towards a better understanding of these systems. River discharge, drainage area, sediment supply, tectonic uplift, rock strength, and grain size can all be modified in our modeling framework to capture characteristics specific to a single landscape. Through thoughtful selection of these variables, our model could be calibrated to represent specific landscapes to correct for biases in measured incision rates and to improve the utility of strath terraces as climate archives.

7. Conclusions

Our numerical modeling framework predicts timing of strath terrace abandonment as a function of the combined impact of fluvial mechanics, tectonics, weather, and climate. We find that measurement biases in rates of river incision are driven by the combined forcing of tectonic rock uplift and climate oscillations. These biases are strongest when rock uplift is slow and climate is highly variable over long time periods. Our work builds a new framework that will allow better linkages between field observations of river incision and terrace evolution with predictive numerical models of landscape evolution. The model increases the reliability of

measurements of river incision by providing a path towards direct correcting for incision rate biases and can be applied in studies that aim to reconstruct climate histories from current landscape form.

Acknowledgments

CD was supported by NSF EAR-1727736 and the Department of Defense National Science and Engineering Graduate Fellowship. BJY was supported by NSF EAR-2123412 and NSF EAR-2120211.

Open research (availability statement)

The OTTERpy code used for this study is available via MIT License and developed openly at https://github.com/clarkedelisle/OTTERPy . *Archiving of input files needed to reproduce the model runs and figures contained in the manuscript is underway and will be available via Zenodo upon acceptance.*

References

Campforts, B., Shobe, C. M., Overeem, I., & Tucker, G. E. (2022). The Art of Landslides: How Stochastic Mass Wasting Shapes Topography and Influences Landscape Dynamics. *Journal of Geophysical Research: Earth Surface*, *127*(8), e2022JF006745. https://doi.org/10.1029/2022JF006745

Craddock, W. H., Kirby, E., Harkins, N. W., Zhang, H., Shi, X., & Liu, J. (2010). Rapid fluvial incision along the Yellow River during headward basin integration. *Nature Geosci*, *3*(3), 209–213. https://doi.org/10.1038/ngeo777

Crave, A., & Davy, P. (2001). A stochastic “precipiton” model for simulating erosion/sedimentation dynamics. *Computers & Geosciences*, *27*(7), 815–827. https://doi.org/10.1016/S0098-3004(00)00167-9

Deal, E., Braun, J., & Botter, G. (2018). Understanding the Role of Rainfall and Hydrology in Determining Fluvial Erosion Efficiency. *Journal of Geophysical Research: Earth Surface*, *123*(4), 744–778. https://doi.org/10.1002/2017JF004393

DeLisle, C., & Yanites, B. J. (2023). Rethinking Variability in Bedrock Rivers: Sensitivity of Hillslope Sediment Supply to Precipitation Events Modulates Bedrock Incision During Floods. *Journal of Geophysical Research: Earth Surface*, *128*(9), e2023JF007148. https://doi.org/10.1029/2023JF007148

DiBiase, R. A., & Whipple, K. X. (2011). The influence of erosion thresholds and runoff variability on the relationships among topography, climate, and erosion rate. *Journal of Geophysical Research: Earth Surface*, *116*(F4), F04036. https://doi.org/10.1029/2011JF002095

Exner, F. M. (1920). *Zur physik der dünen*. Hölder.

Exner, F. M. (1925). Uber die wechselwirkung zwischen wasser und geschiebe in flussen. *Akad. Der Wiss in Wien, Math-Naturwissenschafliche Klasse, Sitzungsberichte, Abt IIa*, *134*, 165–203.

Finnegan, N. J., Schumer, R., & Finnegan, S. (2014). A signature of transience in bedrock river incision rates over timescales of 104-107 years. *Nature*, *505*(7483), 391–394. https://doi.org/10.1038/nature12913

Gallen, S. F., Pazzaglia, F. J., Wegmann, K. W., Pederson, J. L., & Gardner, T. W. (2015). The dynamic reference frame of rivers and apparent transience in incision rates. *Geology*, G36692.1. https://doi.org/10.1130/G36692.1

Gardner, T. W., Jorgensen, D. W., Shuman, C., & Lemieux, C. R. (1987). Geomorphic and tectonic process rates: Effects of measured time interval. *Geology*, *15*(3), 259–261. https://doi.org/10.1130/0091-7613(1987)15<259:GATPRE>2.0.CO;2

Gran, K. B., Finnegan, N., Johnson, A. L., Belmont, P., Wittkop, C., & Rittenour, T. (2013). Landscape evolution, valley excavation, and terrace development following abrupt postglacial base-level fall. *GSA Bulletin*, *125*(11–12), 1851–1864. https://doi.org/10.1130/B30772.1

Hancock, G. S., & Anderson, R. S. (2002). Numerical modeling of fluvial strath-terrace formation in response to oscillating climate. *Geological Society of America Bulletin*, *114*(9), 1131–1142. https://doi.org/10.1130/0016-7606(2002)114<1131:NMOFST>2.0.CO;2

Lague, D., Hovius, N., & Davy, P. (2005). Discharge, discharge variability, and the bedrock channel profile. *Journal of Geophysical Research: Earth Surface*, *110*(F4). https://doi.org/10.1029/2004JF000259

Malatesta, L. C., & Avouac, J.-P. (2018). Contrasting river incision in north and south Tian Shan piedmonts due to variable glacial imprint in mountain valleys. *Geology*, *46*(7), 659–662. https://doi.org/10.1130/G40320.1

Marc, O., Behling, R., Andermann, C., Turowski, J. M., Illien, L., Roessner, S., & Hovius, N. (2019). Long-term erosion of the Nepal Himalayas by bedrock landsliding: the role of

monsoons, earthquakes and giant landslides. *Earth Surface Dynamics*, *7*(1), 107–128. https://doi.org/10.5194/esurf-7-107-2019

Meyer-Peter, E., & Müller, R. (1948). Formulas for bed-load transport. IAHR.

Molnar, P., Erik Thorson Brown, Burchfiel, B. C., Deng, Q., Feng, X., Li, J., et al. (1994). Quaternary Climate Change and the Formation of River Terraces across Growing Anticlines on the North Flank of the Tien Shan, China. *The Journal of Geology*, *102*(5), 583–602.

Molnar, P., Anderson, R. S., Kier, G., & Rose, J. (2006). Relationships among probability distributions of stream discharges in floods, climate, bed load transport, and river incision. *Journal of Geophysical Research*, *111*(F2). https://doi.org/10.1029/2005JF000310

Nativ, R., & Turowski, J. M. (2020). Site Dependence of Fluvial Incision Rate Scaling With Timescale. *Journal of Geophysical Research: Earth Surface*, *125*(11), e2020JF005808. https://doi.org/10.1029/2020JF005808

Paola, C., & Voller, V. R. (2005). A generalized Exner equation for sediment mass balance. *Journal of Geophysical Research*, *110*, 8 PP. https://doi.org/200510.1029/2004JF000274

Rittenour, T. M. (2008). Luminescence dating of fluvial deposits: applications to geomorphic, palaeoseismic and archaeological research. *Boreas*, *37*(4), 613–635. https://doi.org/10.1111/j.1502-3885.2008.00056.x

Sadler, P. M. (1981). Sediment Accumulation Rates and the Completeness of Stratigraphic Sections. *The Journal of Geology*, *89*(5), 569–584.

Schanz, S. A., Montgomery, D. R., Collins, B. D., & Duvall, A. R. (2018). Multiple paths to straths: A review and reassessment of terrace genesis. *Geomorphology*, *312*, 12–23. https://doi.org/10.1016/j.geomorph.2018.03.028

Schumer, R., & Jerolmack, D. J. (2009). Real and apparent changes in sediment deposition rates through time. *Journal of Geophysical Research*, *114*, 12 PP. https://doi.org/200910.1029/2009JF001266

Sklar, L. S., & Dietrich, W. E. (2001). Sediment and rock strength controls on river incision into bedrock. *Geology*, *29*(12), 1087–1090. https://doi.org/10.1130/0091-7613(2001)029<1087:SARSCO>2.0.CO;2

Sklar, L. S., & Dietrich, W. E. (2004). A mechanistic model for river incision into bedrock by saltating bed load. *Water Resources Research*, *40*(6), n/a-n/a. https://doi.org/10.1029/2003WR002496

Stock, J. D., Montgomery, D. R., Collins, B. D., Dietrich, W. E., & Sklar, L. (2005). Field measurements of incision rates following bedrock exposure: Implications for process controls on the long profiles of valleys cut by rivers and debris flows. *Geological Society of America Bulletin*, *117*(1–2), 174–194. https://doi.org/10.1130/B25560.1

Tao, Y., Xiong, J., Zhang, H., Chang, H., & Li, L. (2020). Climate-driven formation of fluvial terraces across the Tibetan Plateau since 200 ka: A review. *Quaternary Science Reviews*, *237*, 106303. https://doi.org/10.1016/j.quascirev.2020.106303

Wegmann, K. W., & Pazzaglia, F. J. (2002). Holocene strath terraces, climate change, and active tectonics: The Clearwater River basin, Olympic Peninsula, Washington State. *Geological Society of America Bulletin*, *114*(6), 731–744. https://doi.org/10.1130/0016-7606(2002)114<0731:HSTCCA>2.0.CO;2

Whipple, K. X., Hancock, G. S., & Anderson, R. S. (2000a). River incision into bedrock: Mechanics and relative efficacy of plucking, abrasion, and cavitation. *Geological Society of America Bulletin*, *112*(3), 490–503. https://doi.org/10.1130/0016-7606(2000)112<490:RIIBMA>2.0.CO;2

Whipple, K. X., Hancock, G. S., & Anderson, R. S. (2000b). River incision into bedrock: Mechanics and relative efficacy of plucking, abrasion, and cavitation. *Geological Society of America Bulletin*, *112*(3), 490–503. https://doi.org/10.1130/0016-7606(2000)112<490:RIIBMA>2.0.CO;2

Wong, M., & Parker, G. (2006). Reanalysis and Correction of Bed-Load Relation of Meyer-Peter and Müller Using Their Own Database. *Journal of Hydraulic Engineering*, *132*(11), 1159. https://doi.org/10.1061/(ASCE)0733-9429(2006)132:11(1159)

Yanites, B., Tucker, G., Mueller, K., Chen, Y., Wilcox, T., Huang, S., & Shi, K. (2010). Incision and channel morphology across active structures along the Peikang River, central Taiwan: Implications for the importance of channel width. *GEOLOGICAL SOCIETY OF AMERICA BULLETIN*, *122*(7–8), 1192–1208. https://doi.org/10.1130/B30035.1

Yanites, B. J. (2018). The Dynamics of Channel Slope, Width, and Sediment in Actively Eroding Bedrock River Systems. *Journal of Geophysical Research: Earth Surface*, *123*(7), 1504–1527. https://doi.org/10.1029/2017JF004405

Yanites, B. J., Tucker, G. E., Mueller, K. J., & Chen, Y.-G. (2010). How rivers react to large earthquakes: Evidence from central Taiwan. *Geology*, *38*(7), 639–642. https://doi.org/10.1130/G30883.1